# Role of oxygen vacancies on light emission mechanisms in $SrTiO_3$ induced by high-energy particles

M. L. Crespillo[1*], J. T. Graham[2,1], F. Agulló-López[3], Y. Zhang[4,1] and W. J. Weber[1,4*]

[1] *Department of Materials Science and Engineering, University of Tennessee, Knoxville, TN 37996, USA*

[2] *Department of Mining and Nuclear Engineering, Missouri University of Science and Technology, Rolla, Missouri 65409, USA*

[3] *Centro de Microanálisis de Materiales, CMAM-UAM, Cantoblanco, Madrid 28049, Spain*

[4] *Materials Science and Technology Division, Oak Ridge National Laboratory, Oak Ridge, TN 37831, USA*

*Corresponding authors:

Email address: mcrespil@utk.edu (M. L. Crespillo) Tel: +1-865-360-2287

Email address: wjweber@utk.edu (W. J. Weber) Tel: +1-865-974-0415

**Abstract**

Light emission under MeV hydrogen and oxygen ions in stoichiometric $SrTiO_3$ are identified at temperatures of 100 K, 170 K and room-temperature. MeV ions predominately deposit their energies to electrons in $SrTiO_3$ with energy densities orders of magnitude higher than from UV or X-ray sources but comparable to femtosecond lasers. The ionoluminescence (IL) spectra can be resolved into three main Gaussian bands at 2.0 eV, 2.5 eV and 2.8 eV, whose relative contributions strongly depend on irradiation temperature, electronic energy loss and irradiation fluence. Two main bands, observed at 2.5 eV and 2.8 eV, are intrinsic and associated with electron-hole

recombination in the perfect $SrTiO_3$ lattice. The 2.8 eV band is attributed to recombination of free (conduction) electrons with an in-gap level, possibly related to self-trapped holes. Self-trapped excitons (STEs) are considered suitable candidates for the 2.5 eV emission band, which implies a large energy relaxation in comparison to the intrinsic edge transition. The dynamics of electronic excitation, governs a rapid initial rise of the intensity; whereas, accumulated irradiation damage (competing non-radiative recombination channels) accounts for a subsequent intensity decrease. The previously invoked role of isolated oxygen vacancies for the blue luminescence (2.8 eV) does not appear consistent with the data. An increasing well-resolved band at 2.0 eV dominates at 170 K and below. It has been only previously observed in heavily strained and amorphous $SrTiO_3$, and is, here, attributed to transitions from $d(t_{2g})$ conduction band levels to $d(e_g)$ levels below the gap. In accordance with *ab-initio* theoretical calculations they are associated to trapped electron states in relaxed $Ti^{3+}$ centers at an oxygen vacancy within distorted $TiO_6$ octahedra. The mechanism of defect evolution monitored during *real-time* IL experiments is presented. In conclusion, the light emission data confirm that IL is an useful tool to investigate lattice disorder in irradiated $SrTiO_3$.

**Keywords:** Ion beam induced luminescence; ionoluminescence; swift ion beam irradiation; irradiation effects; high dense electronic excitation; strontium titanate

**PACS:** Atomic beams interactions with solids, 79.20.Rf; Irradiation effects in solids, 61.80.-x; Titanates, 77.84.Cg; Defects, crystal, 61.72.-y; Electronic excitation and ionization atomic collisions, 34.50.Fa; Electronic structure interaction effects on, 31.70.-f; Electron-ion scattering excitation and ionization, 34.80.-I; Excitons, 71.35.-y; ionoluminescence, 78.60.Hk; Spectroscopy of solid state dynamics, 78.47.-p

*Corresponding authors:

Department of Materials Science and Engineering, University of Tennessee, Knoxville, TN 37996, United States. Ph: +1-865-360-2287. Email address: mcrespil@utk.edu (M. L. Crespillo).

Department of Materials Science and Engineering, University of Tennessee, Knoxville, TN 37996, United States. Ph: +1-865-974-0415. Email address: wjweber@utk.edu (W. J. Weber)

## 1. Introduction

Perovskite oxides are a fascinating class of materials with an extraordinary variety of physical properties. In particular, stoichiometric $SrTiO_3$ (STO) is an insulator with a simple cubic structure exhibiting an indirect band-gap of 3.2 eV at RT, and second-order phase transitions at low temperatures (20, 35 and 105 K) [1].The electrons are highly mobile at low temperature, leading to metallic behavior and superconductivity below 1.2 K [2-5]. Owing to the high permittivity of STO, electronic carriers can strongly couple to the highly polarizable crystal lattice and become self-trapped in the form of small polarons. In particular, holes have been recently shown to self-trap in the lattice at $O^-$ sites surrounded by a distorted lattice [6]. The calculated self-trapping energy is 13 meV, and the energy barrier for polaron hopping is 66 meV, leading to a low hole mobility ($5.09\times10^{-3}$ $cm^2/Vs$) at room-temperature (RT). On the other hand, while electron self-trapping has been observed in many oxides including $LiNbO_3$ [7] and $PbTiO_3$ [8], there is a lack of experimental evidence for self-trapping in $SrTiO_3$, although this possibility has been previously considered [9, 10]. In fact, a self-trapped electron as $Ti^{3+}$ was proposed to be responsible for a donor level at 0.6 eV below the conduction band minimum, observed after X-ray irradiation [10] and by UV photoemission spectroscopy [9].

Aside from transport properties, luminescence experiments in the regime of electronic excitation density are a powerful tool to investigate electron (e) and hole (h) trapping and e-h recombination processes. So far, a variety of irradiation sources have been used for electronic excitation including pulsed laser excitation, photoluminescence, X-rays, and electrons (cathodoluminescence, CL). The main objective has been to correlate the optical emission bands with in-gap electron and hole levels associated to either intrinsic or extrinsic recombination centers.

Interpreting the available experimental information is difficult since it represents combinations of different types of samples (stoichiometric, non-stoichiometric, Nb-doped, acceptor-doped, reduced in low-oxygen pressure, ion (Ar)- irradiated, amorphous, etc), different excitation sources (UV light, laser pulses, electrons) and different temperatures. The basic situation summarized in **Table I** shows that practically all previously performed experiments use light excitation above the band gap. In addition to a band-edge emission at 3.2 eV for temperatures below 100 K [11], the results in **Table I** indicate that, the emission spectra cover an extended wavelength range and include components at 2.0 eV, 2.4-2.5 eV, and 2.9 eV, depending on material and irradiation conditions. In particular, the relative intensities of the bands depend on *n* or *p*-type doping or prior ion irradiation, as well as excitation spectra and density. The band at 2.0 eV is difficult to identify, and it appears as an unresolved shoulder to the other bands. It has been attributed by some authors to light emission in heavily strained or amorphous STO [12-15].

The interpretation of the various identified components of the emission spectra is still controversial. A main point of controversy relates to the competition between intrinsic and extrinsic recombination mechanisms for light emission and, particularly, with the role of oxygen vacancies, which are the most investigated lattice defect. Kan *et al.* [16] have proposed that e-h recombination at oxygen vacancies accounts for the blue emission at 2.8 eV, whereas the green emission at 2.4 eV has been attributed to intrinsic self-trapped exciton (STE) recombination [10, 17]. On the other hand, Rubano *et al.* [17] have proposed that the two green and blue bands are both intrinsic and associated with different e-h recombination pathways. Another point to be clarified is the role of self-trapped electrons (or holes) and self-trapped excitons (STEs), which may be stabilized by local lattice distortions due to strong electron-phonon coupling [3, 18].

To the best of our knowledge, experiments have not yet been performed using electronic excitation with ion beams (ion beam induced luminescence or ionoluminescence, IL), although there are a number of luminescence measurements on samples previously irradiated with ions [19]. IL experiments are not a simple variant of those ones using light excitation or photoluminescence (PL). They constitute an *in-situ* real-time technique that, depending on ion mass and energy, offers a wide range of penetration depths, excitation schemes (see **Section 4. Discussion**) and excitation densities. In particular, high-energy ions (E > 0.1 MeV/amu), where energy is mostly deposited to electrons in the material causing electronic excitation, offer interaction time and excitation density similar to those achieved through high-power femtosecond (fs) pulsed-laser excitation. Moreover, the damage to the lattice caused by either electronic excitation or elastic ion-atom scattering (nuclear energy loss) allows introducing controlled amounts of lattice defects, mainly vacancies and interstitials. Furthermore, the penetration depth can be varied from less than one micron to tens of microns, through an appropriate choice of ion energy; thus, in contrast to low energy CL or UV light excitation, surface effects can be minimized [20-22]. One advantage of IL [23, 24] is that, being an *in-situ* technique, it avoids post-irradiation annealing processes that may modify the structural evolution brought about by the irradiation.

The purpose of this work is to carry out ion-beam irradiation experiments using high-energy ions (H and O), where the dominant interaction with the material is electronic. In a way, these experiments appear similar to those performed by Rubano et *al.* [17, 25] with photon energies above the band-gap of STO (3.2 eV). In fact, the excitation densities are similar and the de-excitation processes may be discussed within a rather common scheme. The role of irradiation fluence has been investigated in the range from $10^{11}$ to $10^{15}$ $cm^{-2}$, and three irradiation temperatures have been used (100 K,

170 K and RT). This extended fluence range offers a transition from a purely electronic excitation in a perfect crystal at low fluences (<$10^{13}$ $cm^{-2}$), to a severely distorted STO lattice due to the oxygen disorder caused at the higher fluences (>$10^{13}$ $cm^{-2}$). These values offer a wide span of physical situations that enable a systematic understanding of the electronic and luminescence processes during ion-solid interaction.

## 2. Experimental details

High-purity stoichiometric STO (100) single crystals, provided by MTI Corporation, were used in this study. One-side polished samples with dimensions of 12.5×12.5×0.5 mm were irradiated at temperatures of 100 K, 170 K and RT under a vacuum of $5\times10^{-5}$ Pa, at the Ion Beam Materials Laboratory (UT-ORNL IBML) at the University of Tennessee, Knoxville [26]. All of the measurements were carried out with the polished side facing both the ion beam and the viewport coupled to the optical fiber used to collect the emitted light (IL). The samples were tilted a few degrees with respect to the incident ion beam to avoid ion channeling. Adjustable beam slits were used to define an irradiation area of 3×3 $mm^2$ (RT) and 2×2 $mm^2$ (100 K, 170 K) on the sample surface. Beam homogeneity was within 10% throughout the irradiated area. Irradiations were performed with 3 MeV H and 8 MeV O with beam current densities in the range of 3-4.5 $nA/mm^2$ to avoid beam heating and charge accumulation on the samples [27]. The ion flux was kept constant throughout each irradiation. For the 3 MeV H irradiations, the ion fluxes were $1.9\times10^{12}$ and $2.8\times10^{12}$ $cm^{-2}s^{-1}$ for the low temperature (LT) and RT irradiations, respectively. For the 8 MeV O irradiations the fluxes were $0.8\times10^{12}$ $cm^{-2}s^{-1}$ and $1.1\times10^{12}$ $cm^{-2}s^{-1}$ for LT and RT irradiations, respectively. Stopping powers for the given ions and materials used in this work were calculated using the Stopping and Range of Ions in Matter (SRIM) binary collision approximation (BCA) software using full-cascade simulations (version 2012) [28, 29]. The calculated stopping

powers are shown in **Table II**, assuming threshold displacement energies of 53.5 eV, 65 eV and 35.7 eV for the Sr, Ti and O atoms, respectively [30], and a density of 4.81g $cm^{-3}$ for STO.

A schematic diagram of the *in-situ* luminescence experimental setup is shown in **Fig. 1** [24]. The light emitted from the samples is transmitted through a sapphire window port at 150° with respect to the ion beam direction, collected into a silica optical fiber of 1 mm diameter located outside of the vacuum chamber and coupled to an imaging spectrometer. The spectral resolution is better than 0.2 nm. More details regarding the optical setup, spectrometer and detector can be found elsewhere [24, 26].

Time evolution of the IL spectra was acquired using an integration time per spectrum between 0.2 and 1.0 s for the case of 3 MeV H at LT and RT, respectively, and 0.1 s in the case of irradiations with 8 MeV O ions. The ion-induced luminescence intensity was normalized to take into account the ion energy, flux, the acquisition time and the irradiated spot area (luminescent area), with the aim of quantitatively comparing the luminescent yields coming from different ion beam irradiations. Therefore, the normalized yields presented here may be considered proportional to the photons per excited electron-hole (e-h) pair. Furthermore, as has been described previously [24], the IL corrected spectra have been converted from wavelength (originally in units of $I(\lambda)d\lambda$) to energy space ($I(E)dE$) by taking into account the factor $\lambda^2$.

The steady state temperature of the sample surface was measured via a K-type (chromel-alumel) thermocouple (TC). More details on the experimental apparatus are provided elsewhere [26, 27].

## 3 Results and analysis

### 3.1 IL Spectra

**Figure 2** (**a, b** and **c**) shows the IL spectra obtained under irradiation with 3 MeV H ions at temperatures of 100 K, 170 K and RT to different ion fluences. Similar experiments were performed at the same temperatures using 8 MeV O, and the measured spectra are displayed in **Fig. 3 (a, b, c**). Essentially, the same bands are observed with O ions as with H ions, although the normalized intensities are higher for O ions in accordance with the higher electronic stopping power (hence higher excitation density). In fact, simple estimates based on the number of generated e-h pairs per ion ($N_{e\text{-}h}$ = E/(2.5×$E_G$), with $E_G$ being the gap energy) and the value of the projected range yield e-h pair densities ($\rho_{e\text{-}h}$) that are roughly 40 times higher for O ions than for H ions (**Table II**). All spectra can be decomposed into three Gaussian bands peaked at around 2.0 eV, 2.5 eV and 2.8 eV, as illustrated in **Fig. 4 (a, b, c)** for the three temperatures and representative fluences. **Table III** provides the peak positions and widths (Full Width at Half Maximum, FWHM) determined for each case. **Figures 2** to **4** clearly show that, for both H and O ion irradiations, the emission yields strongly increase with decreasing temperature. In addition, one notices that for both ions the 2.0 eV emission dominates at low temperatures (around or below 100 K); whereas at RT, the 2.5 and 2.8 eV bands are predominant and the 2.0 eV band appears as a shoulder. It is remarkable that the clearly identifiable and resolved emission band at 2.0 eV has not been previously reported.

### 3.2 Kinetics of emission yield with irradiation fluence

For H irradiations, the dependence of the peak emission yields (area under the Gaussian fit) on ion fluence for each band and temperature is shown in **Fig. 5 (a)** for the

2.5 eV and 2.8 eV bands, and in **Fig. 5 (b)** for the band at 2.0 eV. The fluence range extends up to $5\times10^{14}$ $cm^{-2}$. Similar information for the case of O ion irradiations is given in **Fig. 6 (a-c)** for fluences up to $2\times10^{14}$ $cm^{-2}$. The inset shows the kinetics of the very low fluence region below $10^{12}$ $cm^{-2}$. The figures show that the yield for the 2.5 eV and 2.8 eV bands exhibits a fast rise (not resolvable by the acquisition time) up to a maximum value followed by a slower decay, this behavior becomes more clearly evident for the O ion irradiations. For H ion irradiations, the decay is hardly observable and the evolution of the yield is essentially flat. Therefore, the experimental behavior is better visualized for the O irradiations. For these irradiations, the key point is that all bands reach a maximum at a fluence of around $10^{11}$ $cm^{-2}$, independent of temperature. On the other hand, for H ions, the rise time in units of fluence is much lower, around $10^{13}$ $cm^{-2}$. This behavior is, in accordance with the much higher excitation rate reached with the O irradiations (see **Section 4. Discussion**). Another noteworthy feature is that the kinetics and absolute yield values for the 2.5 eV and 2.8 eV bands are quite similar.

As to the band observed at 2.0 eV, it shows a different behavior to that for the 2.5 and 2.8 eV bands. The initial rise of the yield at low fluences is much slower and significant values are only reached at high enough fluences where the irradiation has caused substantial disorder. In accordance with this view, the rise of the yield is considerably enhanced for oxygen ion irradiation due to the higher damage rate.

## 4 Discussion

The experimental approach provides an extensive set of data across a wide range of excitation densities and irradiation temperatures, heretofore not studied. The spectral and kinetic data obtained in the present work, together with those previously obtained (see **Table I**), offer adequate grounds for a meaningful discussion about the mechanisms of the luminescence emissions at 2.0 eV, 2.5 eV and 2.8 eV.

### 4.1. The blue (2.8 eV) and green (2.5 eV) bands

The bands observed at 2.8 eV and 2.5 eV under 170 K and RT irradiations are similar to those obtained for other radiation sources, such as laser pulses or X-rays, where no lattice defects are introduced, and over a variety of crystal sources and qualities. Therefore, this may suggest that the responsible optical transitions are intrinsic and not related to either impurities or irradiation-induced structural defects. Moreover, the kinetic data (**Figs. 5** and **6**) provide strong support to this view. In fact, they show that the yields start from a small value and rapidly develop with irradiation (at low enough fluences) before a substantial amount of defects have even been introduced by the irradiation. In other words, they appear to correspond to optical transitions between electronic states of the excited electron-hole cloud that precedes structural modifications of the crystal. This point can be quantitatively supported by some simple SRIM calculations assuming that the lattice damage arises from elastic nuclear collisions. At the damage peak, the damage rate is $3.1\times10^{-19}$ dpa cm$^2$ for H (3 MeV) and $1.9\times10^{-16}$ dpa cm$^2$ for O (8 MeV) leading to an atomic concentration of possible recombination centers of around $10^{-6}$ for both H and O ions at the peak of the kinetic curve. These concentrations are, in principle, low enough to represent optical transitions from a recombination center (impurity or defect). After the fast initial growth, the kinetic curves experience a very pronounced decay, indicating that the lattice defects generated during irradiation are effectively "quenching" the luminescence emissions. It is noteworthy that the rate of decrease in the case of O irradiations is about a factor of 100 times larger than for H ions, which could be qualitatively consistent with the simple SRIM estimates for the damage production given above. This argument should be validated in future work by comparing the kinetics of a wider range of ions and energies. One should, however, note that in some previous studies it has been proposed

that the active in-gap levels are associated with intrinsic lattice defects, such as oxygen vacancies [16, 31]. It is indeed true that oxygen vacancies are created by the ion-beam irradiation, at least due to elastic nuclear collisions [32]. However, the arguments given above, particularly the very rapid initial rise of the emission yield at very low fluences ($<10^{13}$ $cm^{-2}$) where a low lattice disorder is generated, makes this proposition questionable.

As a consequence of the above results and discussions, one should ascribe the green and blue bands to intrinsic transitions between conduction-band electrons or valence-band holes and "intrinsic" in-gap levels, or alternatively to transitions between levels of self-trapped excitons (STEs). In principle, the simplest candidate for these in-gap levels is the self-trapped hole ($O^-$) [13], whose existence has been previously ascertained [6, 13]. Therefore, we propose that the spectral component at 2.8 eV, which is close to the band-gap energy, could be related to an optical transition from conduction band levels (possibly at the band minima) to such an in-gap level. Theoretical calculations have yielded a self-trapping energy of 0.130 eV above the valence band edge, qualitatively supporting our proposed assignment for the 2.8 eV emission peak. On the other hand, the 2.5 eV emission band, which is very often observed under a variety of excitations and exhibits a larger energy relaxation, may correspond to recombination of self-trapped excitons (STEs), as suggested by a number of authors [8, 10, 17, 25].

In relation to the above discussion, it is interesting to compare the proposed mechanisms for the 2.5 and 2.8 eV bands with some nanosecond-scale kinetic data obtained with a pulsed laser source at RT [17, 25]. The yield of a blue (2.9 eV) emission in STO crystals was monitored under laser excitation above the band gap (3.49 eV). The studies reveal two different behaviors, unimolecular (UD) kinetics, associated with

bound e-h pairs (excitons), and bimolecular kinetics (BD), attributed to transitions from free (conduction) electrons to some in-gap level, such as that provided by the self-trapped hole. This behavior may be consistent with that expected for the contribution of the two bands peaked at 2.5 eV and 2.8 eV, which are strongly mixed. Unfortunately, these previous efforts [17, 25] to identify the spectra of the two kinetic components were unsuccessful, due to the strongly overlapped and unresolved bands.

It is relevant to ask about the role of irradiation temperature on the relative importance of the two emissions. The 2.5 eV band is clearly apparent at low temperatures but its intensity strongly decreases at RT. This could be, indeed, due to the enhancement of non-radiative recombination processes, even thermal annihilation, as revealed by the shortening of the total emission lifetime of the excitation [25]. However, one should also consider the migration of the STEs at high temperatures to certain "killer" traps, which quench the luminescence. In other words, the present data strongly support the previous hypothesis that the 2.8 eV and 2.5 eV emissions correspond to two alternative intrinsic channels: recombination of conduction band electrons with self-trapped holes for the 2.8 eV band and to STEs for the 2.5 eV band. It is worth mentioning that the 2.8 eV band may include transitions from excited conduction band levels above the band edge in the case of high enough excitation densities and/or temperatures [17, 25]. This could explain some observed asymmetry of the band that extends further into the high-energy side. The simple Gaussian fitting of the present work does not consider asymmetry nor the possible cut-off from the band edge.

### 4.2. The orange (2.0 eV) emission band

The origin of the 2.0 eV emission is less clear and maybe qualitatively different from that proposed for the other two bands. This emission has only been distinctly observed in amorphous or heavily disordered STO, obtained after high temperature

annealing in vacuum [33] or after light-ion irradiations ($H^+$ and $C^-$ at 60 keV) [34]. Theoretical calculations reveal that the disorder associated to O-vacancies introduces new electronic levels in the gap as well as modifies the location of the Fermi level. In fact, it has been shown [35] that *n*- and *p*-doping, associated to the introduction of either O-vacancies or V or Sc substitutional impurities generate new Ti *3d*-$e_g$ states below the conduction band edge. Similar results have also established [36, 37] that O-vacancies induce a chemical reduction of the two Ti ions adjacent to the vacancy so that the two oxygen electrons occupy *3d*-$e_g$ orbitals extending towards the center of the vacancy. As far as we know, direct optical evidence for these levels was not yet available.

In accordance with the above theoretical calculations our proposal is that the 2.0 eV emission band is associated with an optical transition from $d(t_{2g})$ conduction band (CB) levels to a localized $d(e_g)$ orbital in a relaxed $Ti^{+3}$ center close to an oxygen vacancy inside the $TiO_6$ octahedral unit. In support of such view, one should also mention that the wavelength range for such emission at 2.0 eV roughly lies at the location where optical transitions have been reported for octahedral $TiO_6$ clusters in solution [38]. Moreover, the location for such a band coincides with the spectral location of an unresolved absorption band in the spectra of X-ray irradiated samples at very low temperatures [10]. Further evidence for the occurrence of $Ti^{3+}$ after plasma treatment of the samples has been obtained from X-ray fluorescence measurements. The octahedral distortion has been attributed to the increase in the concentration of oxygen vacancies [39]. The band only appears at very low temperatures (100 K), and it rapidly disappears after the end of irradiation, as expected for an electron polaron that may migrate and become trapped at defects or color centers created by the irradiation [40]. The proposed assignment for the 2.0 eV band is also supported by the remarkably higher yield of the emission under O (8 MeV) compared to those obtained under H (3

MeV) irradiation, possibly due to the much higher concentration of oxygen vacancies and higher lattice disorder in the first case. The fact that such a band has not been observed in many previous studies may be due to the use of photoluminescence measurements with very narrow laser light excitation and photon energies slightly above the (direct and indirect) band gaps. In contrast to those experiments, irradiations with charged particles, either via cathodoluminescence (CL) or ionoluminescence (IL), excite a larger span of conduction band levels that should allow the observation of localized *d-d* transitions overlapped with those arising from conduction band states. The influence of the excitation source on the shape and composition of the luminescence spectra is not novel, and it has been illustrated in a recent study [41]. In summary, the origin of the 2.0 eV luminescent band may provide sound evidence for the existence of trapped electrons as relaxed $Ti^{3+}$ centers. As a conclusion, the proposed optical transitions in this work are schematically illustrated in **Fig. 7**.

One may, indeed, think of additional structural characterization experiments to quantify the oxygen concentration in the irradiated samples and provide an independent test for the model. As an example, RBS/C (Rutherford Backscattering Spectroscopy in Channeling configuration) experiments performed previously by authors [42] clearly show the progressive amorphization of the STO crystal with fluence until a fully amorphous state is achieved at damage doses (calculated number of displacements per host atom) reach values from 0.1 to 0.4, depending on the temperature. Unfortunately, these experiments do not distinguish the type of defects, and thus the specific role of oxygen vacancies cannot be separately identified. Therefore, we have performed, as an alternative convenient strategy, some calculations of the vacancy concentrations generated in the initial region of irradiation before clusters and more complex defects are formed. These calculations are based on a SRIM code and use displacement energy

values obtained from molecular dynamics calculations [30]. They show that at fluences of 7.0 x$10^{12}$ $cm^{-2}$ for H and 8.0 x$10^{10}$ $cm^{-2}$ for O similar vacancy concentrations of around $10^{-6}$ (1 appm) are produced; whereas, from the IL kinetic curves, a similar yield around $10^{7}$ a.u. is measured for the 2.0 eV emission in both H and O samples irradiated at 100 K for comparable fluences, respectively. In this fluence range, the oxygen vacancy concentration should increase linearly with fluence, which is consistent with the linear increase in IL yield with fluence at 100 K. A more quantitative correlation of these concentrations with the luminescence yields is not easy, since the quantum efficiency of the corresponding optical transitions responsible for the 2.0 eV band is not known. In summary those SRIM calculations qualitatively support our analysis of IL mechanisms although further work is still needed to assess the proposed model for the 2.0 eV emission band.

## 5. Summary and outlook

Ionoluminescence spectra during ion-beam irradiation with 3 MeV H and 8 MeV O ions have been presented and discussed. They cover a broad spectral range that can be decomposed into three main Gaussian components at 2.0 eV, 2.5 eV and 2.8 eV, whose intensities strongly depend on irradiation conditions (ion mass, energy, temperature and fluence). The effect of irradiation fluence suggests that optical transitions at impurity and/or oxygen-vacancy levels should be ruled out as the origin of the 2.5 eV and 2.8 eV IL emissions. According to the present data and the available information in the literature, the 2.8 eV band appears to be due to transitions from conduction band electrons to intrinsic in-gap levels, very likely associated with self-trapped holes. On the other hand, the 2.5 eV transition, showing a large energy relaxation, may correspond to recombination of a self-trapped excitons (STEs), which are rapidly formed after electronic excitation of the STO lattice. The 2.0 eV band is particularly interesting. The

proposal discussed in this work ascribes it to transitions from CB $d(t_{2g})$ levels to $d(e_g)$ states below the gap, and associated to oxygen vacancies introduced by irradiation. These latter *d* states are localized inside a $TiO_6$ octahedron that becomes distorted by the oxygen vacancies introduced by the irradiation. This mechanism is consistent with previous observations of the same band in strongly strained and amorphous STO. The connection between luminescent emissions and lattice strain, recently ascertained for ion-beam irradiated silica, is a topic of upmost interest [23] and should be further investigated in future work. Furthermore, this work illustrates the relevance of luminescence as an *in-situ*, real-time and highly-sensitive tool for structural characterization of materials.

**Acknowledgements**

This work was supported by the U.S. Department of Energy, Office of Science, Basic Energy Sciences, Materials Sciences and Engineering Division. M. L. Crespillo and J. T. Graham acknowledge support from the University of Tennessee Governor's Chair program.

## Tables

**Table I.** Summary of experimental results from several spectroscopic techniques and excitation sources for emission bands observed in STO.

| **STO samples** | **Excitation source/ Energy** | **Temperature** | **Emission band peak (eV)** | **References** |
|---|---|---|---|---|
| Stoichiometric | ps-laser (3.49 eV) | RT | 2.4, 2.9 | [17] |
| Stoichiometric | electrons (CL) (20 kV/15 nA) | RT | 2.4, 2.9 | [43] |
| Stoichiometric | X-rays (50 kV/40 mA) | LT (15 K) | 2.5 | [10] |
| Stoichiometric | ns-laser (N-He) (3.68 eV) | LT (< 100 K) | 2.5 | [44] |
| Stoichiometric and doped | ps-laser (3.5 eV) | above RT | 2.3, 2.8, 3.0 | [25] |
| O vacancy doping | electrons (CL) (20 kV/15 nA) | RT | 2.4, 2.9 | [43] |
| O vacancy doping | laser (He-Cd) (3.82 eV) | RT | 2.9 | [16] |
| O vacancy doping | laser (He-Cd) (3.82 eV) | LT | 2.4 | [16] |
| Stoichiometric and impurity doping | electrons (CL) | RT | 2.1, 2.4, 2.8 | [39] |
| Acceptor doped, non-doped, amorphous | laser (Ar) (2.41 eV) | RT | 2.1, 2.2 | [12] |
| Stoichiometric, amorphous | laser (Ar) (2.54 eV) | RT | 2.0, 2.4 | [13] |
| Stoich., non-stoichiometric | laser (Ar) (2.54 eV) | RT | 2.0, 2.4 | [14] |
| Stoich., O vacancy doping, amorphous | laser (He-Cd) (3.82 eV) | RT $\rightarrow$ LT (300 - 20 K) | 1.5, 2.0, 2.3 2.5, 2.9, 3.1 | [15] |

**Table II.** Irradiation parameters for the ions and materials used in this work, calculated using Stopping and Range of Ions in Matter (SRIM) full-cascade simulations (version 2012) [28, 29], where $S_e$ is the electronic stopping power at the surface, $S_{e\ max}$ is the maximum value of the electronic stopping power, $S_n$ is the maximum value of the nuclear stopping power and $R_p$ is the projected ion range. $N_{e\text{-}h}$, average number of electron-hole (e-h) pairs generated by single ion impact along the whole trajectory, $\rho_{e\text{-}h}$, e-h pairs density per unit of volume along the ion trajectory considering an excitation radius of ~10 nm.

| Ion | Energy (MeV) | $S_e$ (keV/nm) | $S_{e\ max}$ (keV/nm) | $S_n$ (keV/nm) | $R_p$ (μm) | $N_{e\text{-}h}$ (e-h/ion) | $\rho_{e\text{-}h}$ (e-h/cm$^3$) |
|---|---|---|---|---|---|---|---|
| H | 3 | 0.04 | 0.14 | $4.76\times10^{-5}$ | 54.0 | $3.75\times10^{5}$ | $2.21\times10^{19}$ |
| O | 8 | 3.16 | 3.21 | $5.10\times10^{-2}$ | 3.6 | $9.93\times10^{5}$ | $8.78\times10^{20}$ |

**Table III.** Peak position and width (FWHM) for each temperature of the three emission bands obtained from the decomposition of the IL spectra under 8 MeV O irradiation shown in **Fig. (4).** The values within brackets are less reliable.

| **Temperature** | **Position (eV)** | **FWHM (eV)** |
|---|---|---|
| RT | 2.00 | (0.42) |
| | 2.52 | 0.57 |
| | 2.82 | 0.35 |
| 170 K | 2.00 | (0.56) |
| | 2.53 | 0.58 |
| | 2.83 | 0.48 |
| 100 K | 2.04 | 0.57 |
| | 2.50 | 0.90 |

**Figure captions**

**Fig. 1.** Schematic of the experimental setup for *in-situ* IL measurements adopted from [24].

**Fig. 2.** IL spectra (a.u. equals "arbitrary units") obtained under 3 MeV H ion irradiation at **(a)** room temperature (RT), **(b)** 170 K and **(c)** 100 K to various fluences. The spectra can be decomposed into three Gaussian bands peaked at 2.0 eV, 2.5 eV and 2.8 eV.

**Fig. 3.** IL spectra obtained under 8 MeV O ion irradiation at **(a)** room temperature (RT), **(b)** 170 K and **(c)** 100 K to various fluences. Note that at the lowest temperature **(c)**, an initial rapid increase is observed in the 2.0 eV emission band that reaches a maximum yield at $2.5\times10^{11}$ $cm^{-2}$.

**Fig. 4.** IL spectra and emission bands components under 8 MeV O ion irradiation for the initial irradiation fluences, where the maximum intensity is reached for different temperatures: **(a)** RT, **(b)** 170 K and **(c)** 100 K. The same three Gaussian bands peaked at 2.0 eV, 2.5 eV and 2.8 eV can be observed. The dashed curves represent the emission bands used to decompose the spectra. The solid green line represents the global fit of the spectrum.

**Fig. 5.** Comparison of the yield intensity as a function of 3 MeV H ion fluences at different temperatures for: **(a)** the 2.5 eV and 2.8 eV emission bands; and **(b)** the 2.0 eV emission band.

**Fig. 6.** Comparison of the yield intensity as a function of 8 MeV O ion fluence at different temperatures for: **(a)** the 2.0 eV emission band, **(b)** the 2.5 eV emission band and **(c)** the 2.8 eV emission band. Insets show more details in the low fluence regime.

**Fig. 7.** Schematic for possible mechanisms of the electronic processes involved in the IL for STO. The conduction band (CB) is mainly composed of a *3d* orbital of Ti and the

valence band (VB) is associated with O *2p* states. White and grey circles represent the excited holes and electrons, respectively. **(a)** The 2.8 eV (blue light) emission band is attributed to recombination of conduction electrons with an in-gap level attributed to self-trapped holes; **(b)** the radiative recombination process of excited holes and electrons in a self-trapped excited state (STE) responsible for the green emission band (2.5 eV); and **(c)** the well-defined band at 2.0 eV (orange) observed at LT is attributed to *d-d* transitions (inside $TiO_6$ octahedron) from electrons that are trapped as relaxed $Ti^{3+}$centers.

**Figures**

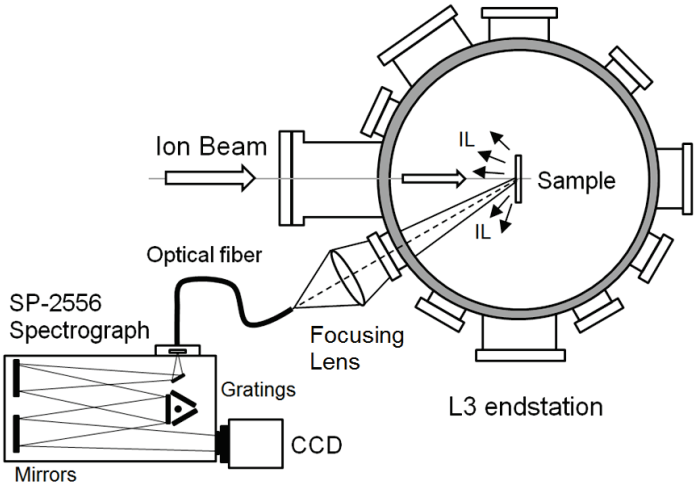


**Fig. 1.**

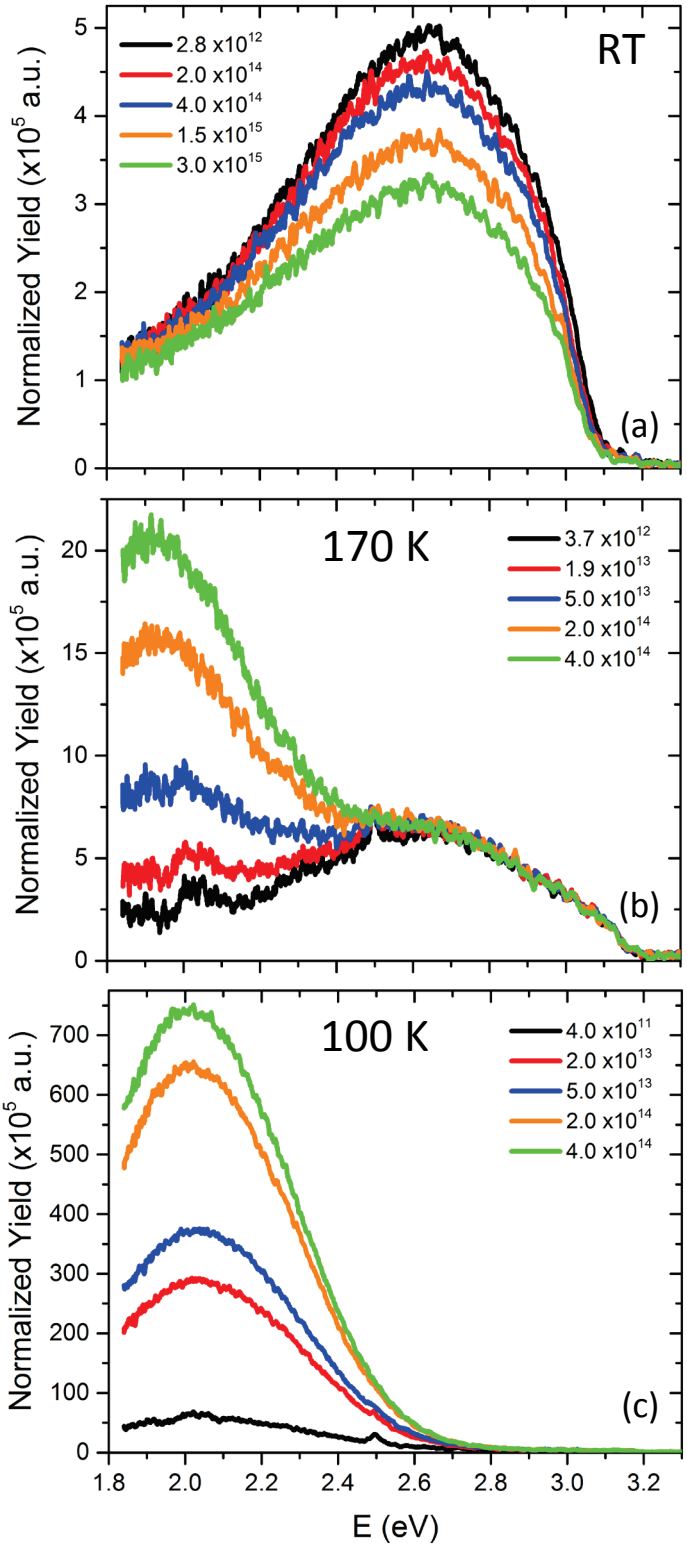
RT
2.8 x10^12
2.0 x10^14
4.0 x10^14
1.5 x10^15
3.0 x10^15
Normalized Yield (x10^5 a.u.)
(a)
170 K
3.7 x10^12
1.9 x10^13
5.0 x10^13
2.0 x10^14
4.0 x10^14
Normalized Yield (x10^5 a.u.)
(b)
100 K
4.0 x10^11
2.0 x10^13
5.0 x10^13
2.0 x10^14
4.0 x10^14
Normalized Yield (x10^5 a.u.)
(c)
E (eV)

**Fig. 2.**

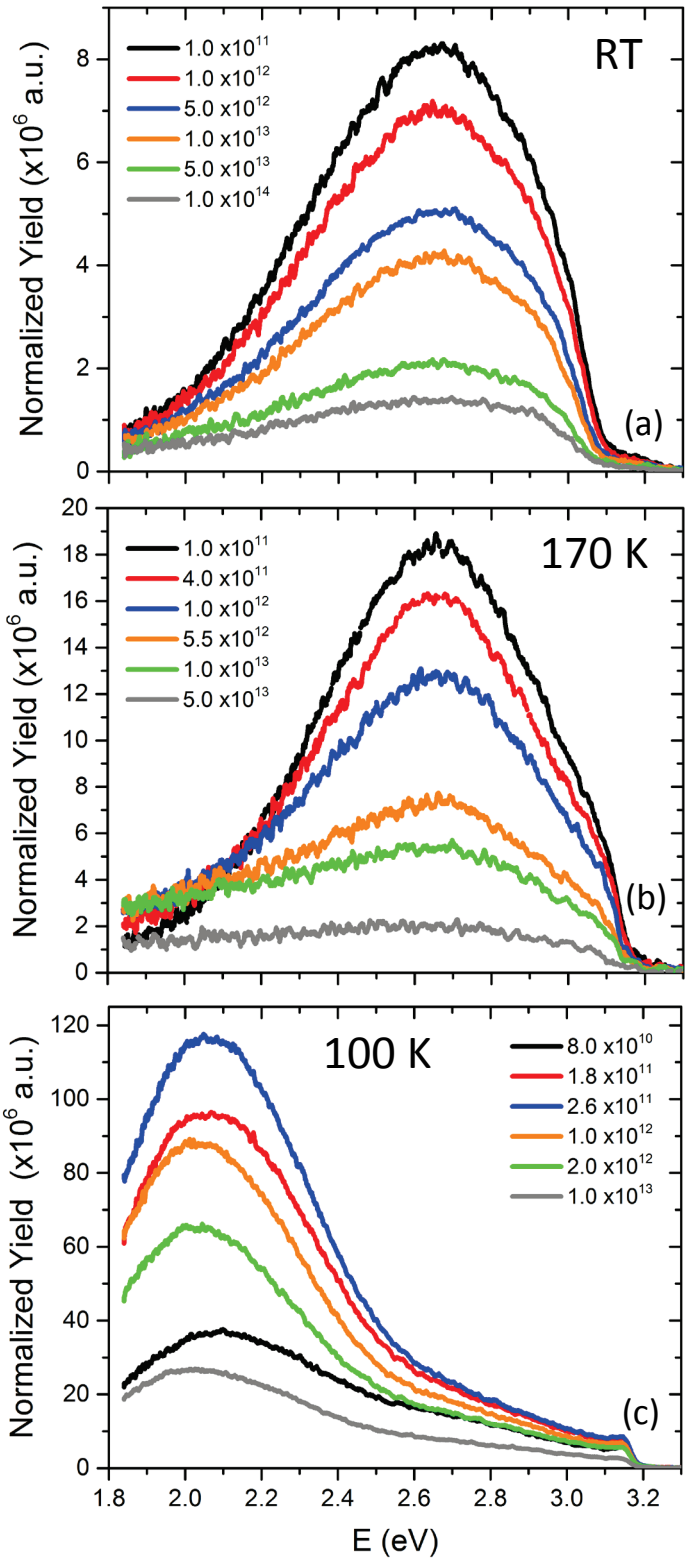
RT
1.0 x10^11
1.0 x10^12
5.0 x10^12
1.0 x10^13
5.0 x10^13
1.0 x10^14
(a)
Normalized Yield (x10^6 a.u.)
170 K
1.0 x10^11
4.0 x10^11
1.0 x10^12
5.5 x10^12
1.0 x10^13
5.0 x10^13
(b)
100 K
8.0 x10^10
1.8 x10^11
2.6 x10^11
1.0 x10^12
2.0 x10^12
1.0 x10^13
(c)
E (eV)

**Fig. 3.**

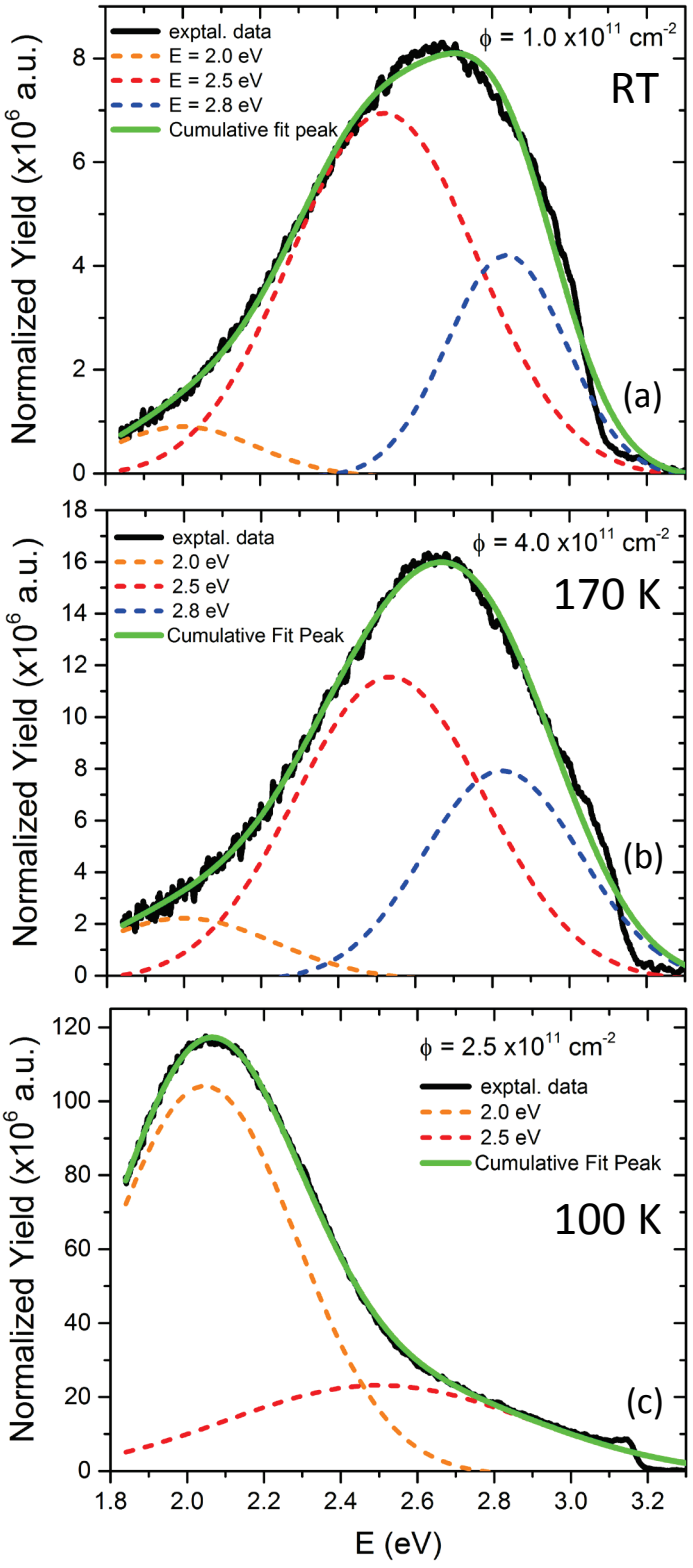
exptal. data
E = 2.0 eV
E = 2.5 eV
E = 2.8 eV
Cumulative fit peak
ϕ = 1.0 x10^11 cm^-2
RT
(a)
Normalized Yield (x10^6 a.u.)
exptal. data
2.0 eV
2.5 eV
2.8 eV
Cumulative Fit Peak
ϕ = 4.0 x10^11 cm^-2
170 K
(b)
ϕ = 2.5 x10^11 cm^-2
exptal. data
2.0 eV
2.5 eV
Cumulative Fit Peak
100 K
(c)
E (eV)

**Fig. 4.**

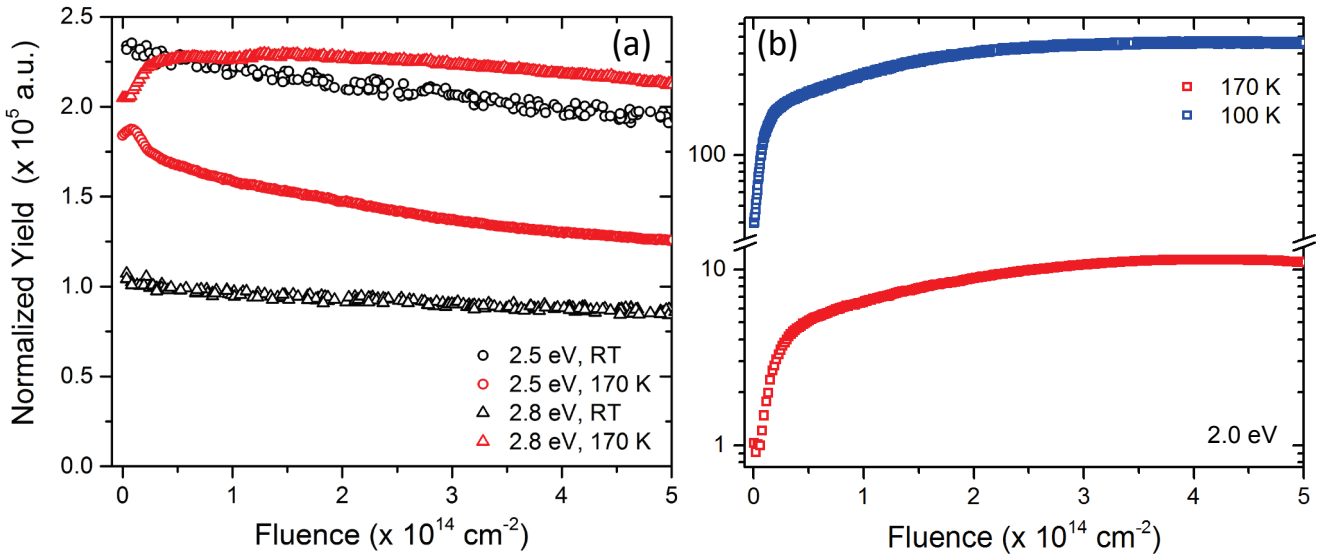
(a)
Normalized Yield (x 10^5 a.u.)
Fluence (x 10^14 cm^-2)
2.5 eV, RT
2.5 eV, 170 K
2.8 eV, RT
2.8 eV, 170 K
(b)
170 K
100 K
2.0 eV
Fluence (x 10^14 cm^-2)

**Fig. 5.**

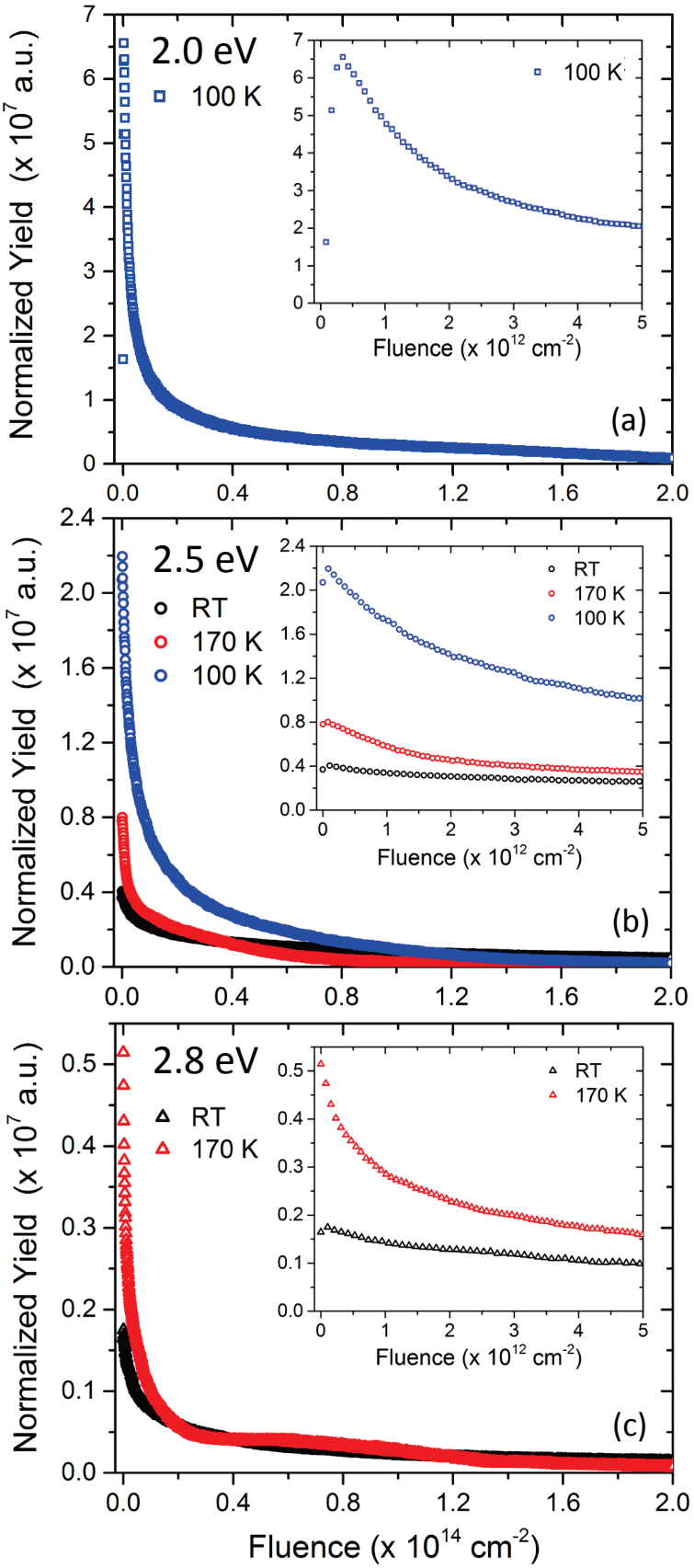
2.0 eV
100 K
Normalized Yield (x 10^7 a.u.)
Fluence (x 10^12 cm^-2)
(a)
2.5 eV
RT
170 K
100 K
(b)
2.8 eV
RT
170 K
(c)
Fluence (x 10^14 cm^-2)

**Fig. 6**

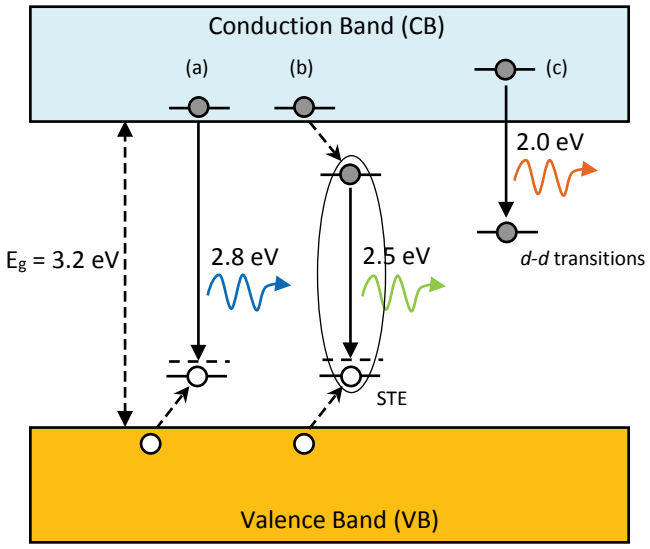
Conduction Band (CB)
(a)
(b)
(c)
2.0 eV
$E_g$ = 3.2 eV
2.8 eV
2.5 eV
*d-d* transitions
STE
Valence Band (VB)

**Fig.7**

## References


[1] Yang B, Townsend P D and Fromknecht R 2004 Low temperature detection of phase transitions and relaxation processes in strontium titanate by means of cathodoluminescence *J. Phys.: Condens. Matter.* **16** 8377-86

[2] Son J, Moetakef P, Jalan B, Bierwagen O, Wright N J, Engel-Herbert R and Stemmer S 2010 Epitaxial $SrTiO_3$ films with electron mobilities exceeding 30,000 $cm^2 V^{-1}s^{-1}$ *Nat. Mater.* **9** 482-84

[3] Keroack D, Lepine Y and Brebner J L 1984 Drift mobility measurements of small-polaron transport in $SrTiO_3$ *J. Phys. C: Solid State Phys.* **17** 833-42

[4] Tufte O N, and Chapman P W 1967 Electron mobility in semiconducting strontium titanate *Phys. Rev.* **155** 796-802

[5] Pellegrino L, Pallecchi I, Marré D, Bellingeri E and Siri A S 2002 Fabrication of submicron-scale $SrTiO_{3-d}$ devices by an atomic force microscope *Appl. Phys. Lett.* **81** 3849-51

[6] Chen H, and Umezawa N 2014 Hole localization, migration and the formation of peroxide anion in perovskite $SrTiO_3$ *Phys. Rev. B* **90** 035202

[7] Schirmer O F, Imlau M, Merschjann C and Schoke B 2009 Electron small polarons and bipolarons in $LiNbO_3$ *J. Phys.: Condens. Matter* **21** 123201

[8] Eglitis R I, Kotomin E A, Trepakov V A, Kapphan S E and Borstel G 2002 Quantum chemical modelling of electron polarons and green luminescence in $PbTiO_3$ perovskite crystals *J. Phys.: Condens. Matter.* **14** L647

[9] Ferrer S, and Somorjai G S 1981 Ultraviolet photoelectron spectroscopy study of the adsorption of oxygen on reduced $SrTiO_3$ surfaces *J. Appl. Phys.* **52** 4792

[10] Aguilar M, and Agulló-López F 1982 X-ray induced processes in $SrTiO_3$ *J. Appl. Phys.* **53** 9009

[11] Yamada Y, and Kanemitsu Y 2012 Band-edge luminescence from $STiO_3$: No polaron effect *Thin Solid Films* **520** 3843-46

[12] Soledade L E B, Longo E, Leite E R, Pontes F M, Lanciotti Jr. F, Campos C E M, Pizani P S and Varela J A 2002 Room-temperature photoluminescence in amorphous $SrTiO_3$-the influence of acceptor-type dopants *Appl. Phys. A* **75** 629-32

[13] Pinheiro C D, Longo E, Leite E R, Pontes F M, Magnani R, Varela J A, Pizanni P S, Boschi T M and Lanciotti F 2003 The role of defect states in the creation of photoluminescence in $SrTiO_3$ *Appl. Phys. A* **77** 81-85

[14] Orhan E, Pontes F M, Santos M A, Leite E R, Beltran A, Andres J, Boschi T M, Pizani P S, Varela J A, Taft C A and Longo E 2004 Combined experimental and theoretical study to understand the photoluminescence of $Sr_{1-x}TiO_{3-x}$ *J. Phys. Chem. B* **108** 9221-27

[15] Kumar D, and Budhani R C 2015 Defect-induced photoluminescence of strontium titanate and its modulation by electrostatic gating *Phys. Rev. B* **92** 235115

[16] Kan D, Terashima T, Kanda R, Masuno A, Tanaka K, Chu S, Kan H, Ishizumi A, Kanemitsu Y, Shimakawa Y and Takano M 2005 Blue-light emission at room temperature from $Ar^+$-irradiated $SrTiO_3$ *Nature Mater.* **4** 816-19

[17] Rubano A, Paparo D, Miletto F, Scotti di Uccio U and Marrucci L 2007 Recombination kinetics of a dense electron-hole plasma in strontium titanate *Phys. Rev. B* **76** 125115

[18] Ang C, Yu Z, Jing Z, Lunkenheimer P and Loidl A 2000 Dielectric spectra and electrical conduction in Fe-doped $SrTiO_3$ *Phys. Rev. B* **61** 3922

[19] Rho J, Jung S, Shin S, Kwon J -H, Yin M, Song J -H and Choi E 2010 Blue and infrared cathodoluminescence induced by carbon-irradiation in $SrTiO_3$ single crystal *J. Lumin.* **130** 1687-89

[20] Townsend P D, Khanlary M and Hole D E 2007 Information obtainable from ion beam luminescence *Surface & Coatings Technology* **201** 8160–64

[21] Townsend P D, and Wang Y 2013 Defect studies using advances with ion beam excited luminescence *Energy Procedia* **41** 64-79

[22] Townsend P D, and Crespillo M L 2016 An ideal system for analysis and interpretation of ion beam induced luminescence *Physics Procedia* **66** 345-51

[23] Bachiller-Perea D, Jiménez-Rey D, Muñoz-Martín A and Agulló-López F 2016 Exciton mechanisms and modeling of the ionoluminescence in silica *J. Phys. D: Appl. Phys.* **49** 085501

[24] Crespillo M L, Graham J T, Zhang Y and Weber W J 2016 In-situ luminescence monitoring of ion-induced damage evolution in $SiO_2$ and $Al_2O_3$ *J. Lumin.* **172** 208-18

[25] Rubano A, Paparo D, Miletto Granozio F, Scotti di Uccio U and Marrucci L 2009 Blue luminescence of $SrTiO_3$ under intense optical excitation *J. Appl. Phys.* **106** 103515

[26] Zhang Y, Crespillo M L, Xue H, Jin K, Chen C -H, Fontana C L, Graham J T and Weber W J 2014 New ion beam materials laboratory for effective investigation of materials modification and irradiation effects *Nucl. Instrum. Meth. B.* **338** 19-30

[27] Crespillo M L, Graham J T, Zhang Y and Weber W J 2016 Temperature measurements during high flux ion beam irradiations *Rev. Sci. Instrum.* **87** 024902

[28] Ziegler J F, Ziegler M D and Biersack J P 2010 SRIM - The stopping and range of ions in matter *Nucl. Instrum. Methods B* **268** 1818-123

[29] Ziegler J F 2012 SRIM v2012 Software code. SRIM -The Stopping and Range of Ions in Matter

[30] Liu B, Xiao H Y, Zhang Y, Aidhy D S and Weber W J 2013 Ab initio molecular dynamics simulations of threshold displacement energies in $SrTiO_3$ *J. Phys.: Condens. Matter.* **25** 485003

[31] Kan D, Kanda R, Kanemitsu Y, Shimakawa Y, Takano M, Terashima T and Ishizumi A 2006 Blue luminescence from electron-doped $SrTiO_3$ *Appl. Phys. Lett.* **88** 191916

[32] Weber W J, Zarkadoula E, Pakarinen O H, Sachan R, Chisholm M F, Liu P, Xue H, Jin K and Zhang Y 2015 Synergy of elastic and inelastic energy loss on ion track formation in $SrTiO_3$ *Sci. Rep.* **5** 7726

[33] Rho J, Jang S, Ko Y D, Kang S, Kim D -W, Chung J -S, Kim M, Han M and Choi E 2009 Photoluminescence induced by thermal annealing in $SrTiO_3$ thin films *Appl. Phys. Lett.* **95** 241906

[34] Rho J-H, and Choi E 2011 Evidence of the primary-color photoluminescence in ion ($H^+$,$H^{2+}$,$C^-$) irradiated and thermal annealed $SrTiO_3$ *J. Lumin.* **131** 69-71

[35] Luo W, Duan W, Louie S G and Cohen M L 2004 Structural and electronic properties of *n*-doped and *p*-doped $SrTiO_3$ *Phys. Rev. B* **70** 214109

[36] Ricci D, Bano G, Pacchioni G and Illas F 2003 Electronic structure of a neutral oxygen vacancy in $SrTiO_3$ *Phys. Rev. B* **68** 224105

[37] Buban J P, Iddir H and Ogüt S 2004 Structural and electronic properties of oxygen vacancies in cubic and antiferrodistortive phases of $SrTiO_3$ *Phys. Rev. B* **69** 180102 (R)

[38] Figgis B N 1966 Introduction to ligand fields (New York: Wiley Interscience)

[39] Kulagin N A, and Hieckmann E 2012 Spectra and color centers of strontium titanate crystals *Optics and Spectroscopy* **112** 79-86

[40] Stoneham A M, Gavartin J, Shluger A L, Kimmel A V, Muñoz Ramo D, Ronnow H M, Aeppli G and Renner C 2007 Trapping, self-trapping and the polaron family *J. Phys.: Condens. Matter* **19** 255208

[41] Wang Y, Zhao Y, Zhang Z, Zhao C, Wu X, Finch A A and Townsend P D 2015 Energy dependence of radioluminescence spectra from strontium titanate *J. Lumin.* **166** 17-21

[42] Zhang Y, J. Lian, C. M. Wang, W. Jiang, R. C. Ewing, and W. J. Weber 2005 Ion-induced damage accumulation and electron-beam-enhanced recrystallization in $SrTiO_3$ *Phys. Rev. B* **72** 094112

[43] Yang K-H, Chen T -Y, Ho N -J and Lu H Y 2011 In-gap states in wide band gap $SrTiO_3$ analyzed by cathodoluminescence *J. Am. Ceram. Soc.* **94** 1811-16

[44] Leonelli R, and Brebner J L 1986 Time-resolved spectroscopy of the visible emission band in strontium titanate *Phys. Rev. B* **33** 8649-56